Self-assembling of Prussian blue nanocubic particles on nanoporous glassy carbon and its use in the electrocatalytic reduction of hydrogen peroxide

Mahmoud Amouzadeh Tabrizi & Anna Alidoost Saharkhiz Lahiji

Journal of the Iranian Chemical Society

ISSN 1735-207X

J IRAN CHEM SOC
DOI 10.1007/s13738-013-0369-3

Springer

J IRAN CHEM SOC
DOI 10.1007/s13738-013-0369-3

ORIGINAL PAPER

Self-assembling of Prussian blue nanocubic particles on nanoporous glassy carbon and its use in the electrocatalytic reduction of hydrogen peroxide

Mahmoud Amouzadeh Tabrizi ·
Anna Alidoost Saharkhiz Lahiji

Received: 30 May 2013 / Accepted: 2 October 2013

Abstract In this paper, self-assembled Prussian blue nanocubic particles on nanoporous glassy carbon was developed. The morphology of the PBNP-modified porous glassy carbon was characterized by scanning electron microscopy. The PBNP-GCE-red film-modified electrode was used for the sensitive detection of hydrogen peroxide. The electrochemical behavior of the resulting sensor was investigated using cyclic voltammetry and chronoamperometry. The value of α, k_{cat}, and D was calculated as 0.35, 1.7×10^5 cm^3 mol^{-1} s^{-1}, and 2.6×10^{-5} cm^2 s^{-1}, respectively. The calibration curve for hydrogen peroxide determination was linear over 0–600 μM with a detection limit (S/N = 3) of 0.51 μM.

Keywords Self-assembly · Nanoporous glassy carbon · Prussian blue nanocubic particles · Hydrogen peroxide · Electrochemical sensor

Introduction

In recent years, the construction and application of modified electrodes has received much attention with a view to the enhancement of sensitivity and selectivity for electroanalytical techniques. The use of metal hexacyanoferrates (MHCF) as redox mediators in modified electrodes has been extensively studied [1–8]. Because of interesting electrocatalytic activity of MHCF for hydrogen peroxide (H_2O_2) such as low potentials, minimizing the interference caused by reductant species, these materials have been widely studied. Rapid and accurate determination of H_2O_2 is of significant importance in many fields including medicine, food industry, biology and environmental protection [9, 10]. Various sensors based on novel metals [11–15], conductive polymers [16–19], and enzymes [20–25] have been reported for fabrication of H_2O_2 sensor in literatures. Unlike these sensors which show limitations such as high cost, lack of sensitivity and susceptibility to interference by other substances in analyte samples, sensors based on Prussian blue (PB) have lower cost, higher selectivity, and easier preparation [26–28]. PB can be reversibly oxidized to Prussian yellow or reduced to Prussian white (PW) so that it acts as an electron transfer mediator (electrocatalyst) for both oxidation and reduction of H_2O_2 [26, 29]. Therefore, the deposition of PB on an electrode surface makes it possible to detect H_2O_2 at a low applied potential; hence, it is possible to eliminate the effect of interfering species [30, 31]. The possibility of selective detection mediated by PB was first demonstrated by Karyakin et al. [32]. Because of many applications of the PB in various fields, a convenient method to immobilize a stable and homogeneous film with controllable morphology on electrode substrate is usually required. Various methods have been developed for the immobilization of PB on the electrode surface, including mechanical attachment [33], adsorption [34], entrapping into polymeric matrices [35], encapsulating into sol–gels [36] and electrodeposition [37]. The most commonly used technique for PB preparation is electrodeposition; however, this technique always produces thick and loose films with poor stability. Self-assembly technique for fabricating film has attracted much

---

Electronic supplementary material The online version of this article (doi:10.1007/s13738-013-0369-3) contains supplementary material, which is available to authorized users.

M. A. Tabrizi (✉) · A. A. S. Lahiji
Department of Chemistry, Institute for Advanced Studies in Basic Sciences, P.O. Box 45195-1159, Gava Zang, Zanjan, Iran
e-mail: mahmoud.tabrizi@gmail.com

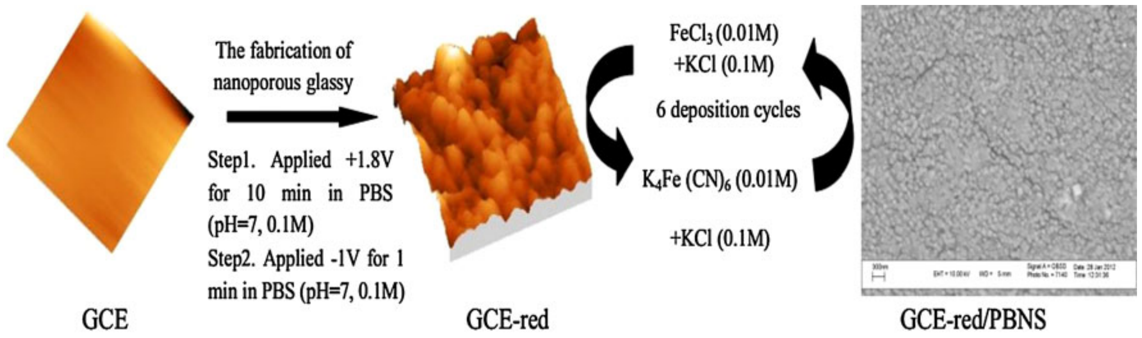

Scheme 1 Preparation of PBNP-GCE-red

interest because of its simplicity in procedure and wide choice of materials [34, 38, 39]. To obtain uniform and defect-free PB thin films, self-assembly process based on multiple sequential adsorption of ferric cations and hexacyanoferrate anions on a charged surface was reported [40–43]. This preparation method for pure PB films provides a precise control of thickness in nano scale by tuning the number of adsorption steps.

Herein, we used a porous substrate for immobilization of PB by self-assembly method. The results showed that a porous film with a large effective area is produced at the reduced glassy carbon electrode (GCE-red) surface. It seems that the porous surface of a GCE-red is a good medium for the self-assembling of PB. Finally, this modification procedure was utilized for construction of a H_2O_2 sensor.

Experimental

Reagents and apparatus

All chemicals were of analytical reagent grade and used without further purification. Double distilled water was used throughout. Standard working solutions of H_2O_2 were prepared freshly by diluting the stock solutions double distilled water.

Cyclic voltammetry and amperometric studies were performed using an Autolab potentiostat–galvanostat model PGSTAT30 (Utrecht, The Netherlands) with a conventional three electrode set-up, in which GCE-red and PBNP-GCE-red, an Ag|AgCl|KCl$_{sat}$ and a platinum rod served as the working, reference and auxiliary electrodes, respectively. Output signal was acquired by Autolab Nova software. Scanning electron microscopy (SEM) was performed with a Philips instrument, Model XL-30 (Eindhoven, The Netherlands). The surface morphology of the GCE-red was characterized using a DME DualScope Scanner DS 95-200 (Herlev, Denmark) atomic force microscopy (AFM).

Results and discussion

Preparation of GCE-red

The GCE-red was prepared according to the method reported previously without modification [44]. In brief, the surface of a GCE with an outer diameter of 3.05 mm was polished successively with 0.3-, 0.1- and 0.05-μm alumina slurry (Struers, Copenhagen, Denmark) and then washed in ethanol and water, respectively, under ultrasonication. A freshly polished GCE was anodized at 1.8 V (versus Ag|AgCl|KCl$_{sat}$) in 0.1 M NaH_2PO_4 for 10 min to obtain a oxidized GCE (GCE-ox). The GCE-ox was then reduced at −1.0 V (versus Ag|AgCl|KCl$_{sat}$) in 0.1 M NaH_2PO_4 for 1 min to obtain a GCE-red [45]. The obtained AFM images of GCE (a) and GCE-red (b) are shown in Fig S1. The surface of GCE-red was quite porous in comparison with the smooth surface of the GCE. The maximum height of the roughness profile and root-mean-square deviation of the roughness profile for the GCE-red were 61.7 and 7.01 nm, respectively. In contrast, these values were 2.46 nm and 738 pm for the polished GCE.

Preparation of Prussian blue nano particles (PBNP)

For the PBNP films, two solutions were prepared. Solution 1: 0.01 M $FeCl_3$ + 0.1 M KCl. Solution 2: 0.01 M $K_4[Fe(CN)_6]$ + 0.1 M KCl. The pretreated electrode was consecutively dipped into solution A, pure water, solution B, and pure water again. The dipping time in solutions A and B was 20 min each, and the washing time in pure water was 1 min. The six steps are denoted as a deposition cycle, and they lead to the adsorption of a single Metal PB layer. After some deposition cycles, the PB-modified electrode was dried at 60 °C for 1 h [40]. The preparative procedure of porous glassy carbon electrode and subsequent PBNs mutilayers assembly processes are shown in Scheme 1.

Characterization of PBNP

The structure of PBNPs was observed by SEM. From Fig. 1, we can see lots of cubic PBNP were distributed on the GCR-red surface uniformly and the average size of PBNP was estimated at 100 nm.

Figure 2 shows cyclic voltammograms (CVs) of PBNP-modified electrodes deposited with various layers. The set of peaks corresponds to redox conversion between PB and its reduced form, PW. With increasing the number of deposition cycles, peak current increased gradually because of the increase of PB loadings; on the other hand, peak separation also increased, indicating the electron transfer slowed down due to the increased thickness of PB film. Figure 3a shows the cyclic voltammograms of the PB and its three analog-modified electrode at different scan rates in 0.1 M KCl solution. The linear dependence of the peak currents, I_{pa} and I_{pc} on the scan rate (v) of potential was obtained up to 300 mV s^{-1} for the first set peaks. This behavior is what expected for surface redox reactions (Fig. 3b). At higher sweep rates, the plot of peak current versus scan rate deviates from the linearity and the peak currents become proportional to the square root of the scan rate indicating diffusion-controlled processes, which can be related to the relatively slow diffusion of counter ions into a limited reaction layer. Because the electrochemical reaction needs the counter ions to balance the charge to maintain the neutrality of the PB during the sweep process, and the migration of the counters K^+ has to pass through the channel of PB for the electrochemical reaction of the inner atoms, therefore the reaction resistance of the inner atoms is larger than that of the surface atoms at the high scan rates, which turns out the incomplete electrochemical reaction. The ratio of current peaks (I_{pa}/I_{pc}) remains almost equal to unity at different scan rates, as expected for surface-type behavior. The surface concentration of the electroactive mediator (Γ) on the electrode surface can be calculated from the slope of the I_{pa} vs. scan rate plot. For a reversible surface reaction, the peak current has been given by the following equation $I_p = n^2F^2vA\Gamma/4RT$ [46]. v is potential sweep rate, A the geometric surface area and other symbols have their usual meanings. The value of ca. 1.0749×10^{-9} mol cm^{-2} was calculated for the PBNP-GCE-red.

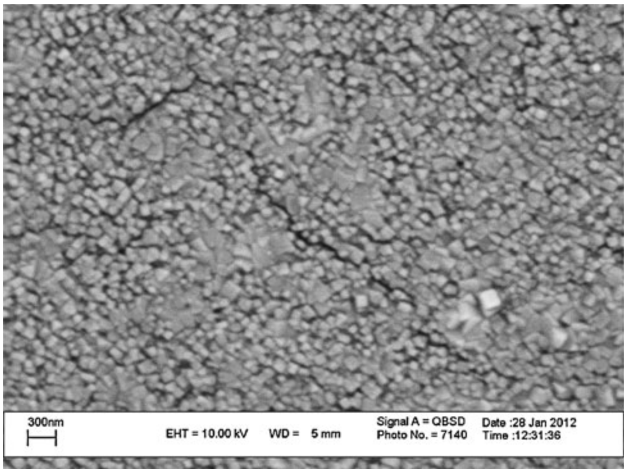

Fig. 1 SEM images of self-assembled PBNP with six deposition cycles at the GCE-red

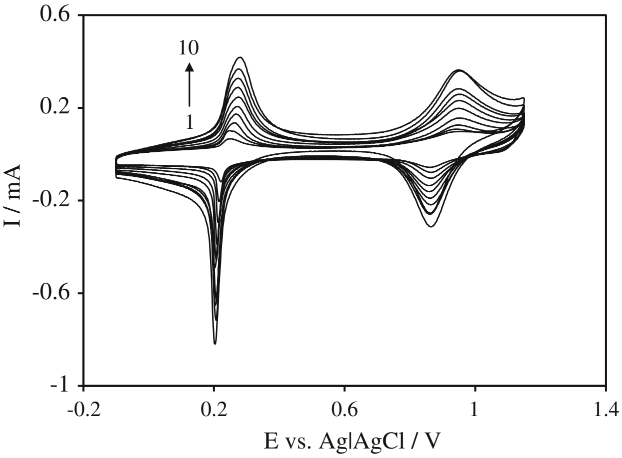

Fig. 2 Cyclic voltammograms of PBNP-modified electrodes with 1, 2, 3, 4, 5, 6, 7, 8, 9 and 10 deposition cycles. The scan rate is 20 mV/s

The Tafel slope can be obtained by another method according to the following equation that is valid for a totally irreversible diffusion-controlled process [47]: $E_p = b/2\ \log(\upsilon) +$ constant where b indicates the Tafel slope. According to this equation, the evaluated slope of Ep vs. log(υ) is 0.0835 V $decade^{-1}$; therefore, $b = 0.\ 167$ V $decade^{-1}$. Hence the amount of α was estimated 0.35.

The redox peak currents decrease with increasing pH of solution. The lack of peaks at higher pH attributed to the interaction between PBS and hydroxyl ions in the solution, which form $Fe(OH)_3$ at pH higher than 4 (Fig. S2). In addition, the various alkali supporting electrolytes solutions including LiCl, NaCl and KCl were separately used as supporting electrolytes, and cyclic voltammogram of the modified electrode was recorded in each solution (0.1 M) at scan rate of 50 mV s^{-1} (Fig. S3). The redox peaks PBNPs at KCl solution as supporting electrolyte exhibits higher current than the others, because K^+ could penetrate into the lattice of PBNPs. Therefore, KCl is selected as a supporting electrolyte for this present study.

Chronoamperometry was used for the evaluation of the catalytic reaction rate constant (k_{cat}) for the chemical reaction between H_2O_2 and redox sites of surface confined PBNP-GCE-red using the following equation [48]. $I_{cat}/I_L = \pi^{1/2}\ (k_{cat}C_ot)^{1/2}$. I_{cat} is the catalytic current of the

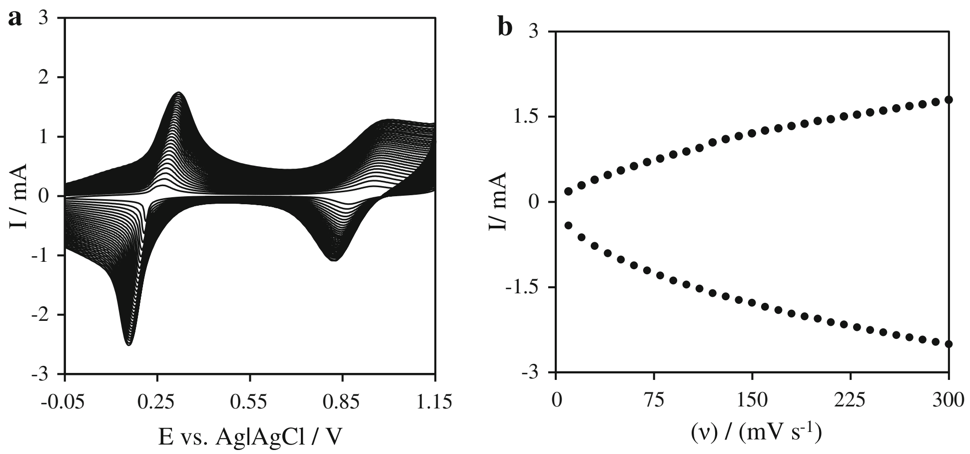

Fig. 3 Typical cyclic voltammograms of the PBNP-GCE-red in 0.1 M KCl (pH 4) solution at various scan rates (from inner to outer curve): 10–300 mV s^{-1} (**a**). Plot of peak current vs. scan rate for the first set peaks (**b**)

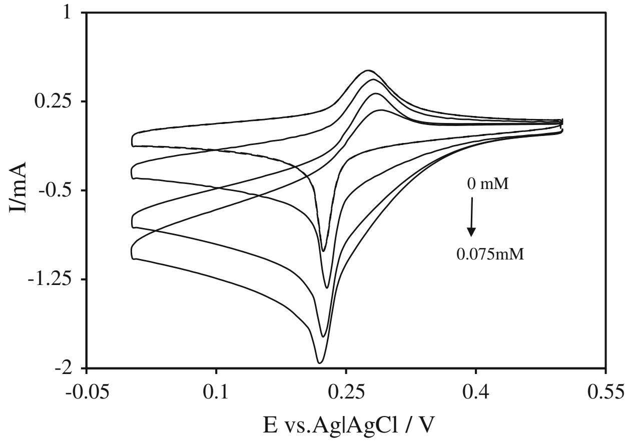

Fig. 4 Cyclic voltammograms of the PBNP-GCE-red in 0.1 M KCl (pH 4) at various concentration of H_2O_2 0, 0.025, 0.05 and 0.075 mM, potential scan rate 20 mV s^{-1}

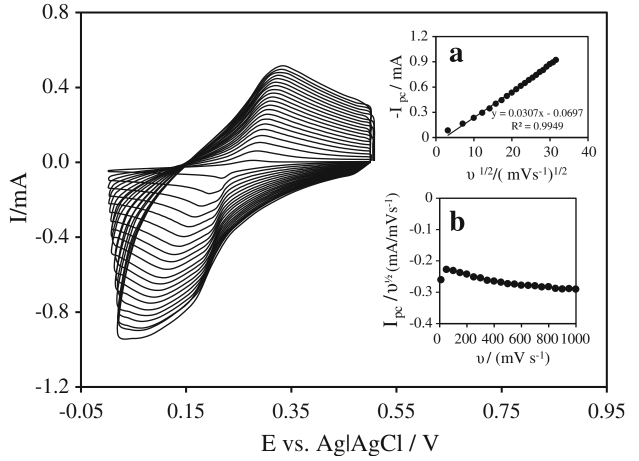

Fig. 5 Cyclic voltammograms of the PBNP-GCE-red in the presence of 0.05 mM H_2O_2. Potential scan rates 10, 100, 200, 300, 400, 500, 600, 700, 800, 900 and 1,000 mV s^{-1}. Insets (**a**) and **b** represent the variations of the cathodic peak current, I_{pc} vs. $v^{1/2}$, and cathodic current function, $I_{pc}/v^{1/2}$ vs. v, respectively

PBNP-GCE-red in the presence of H_2O_2, I_L is the limiting current in the absence of H_2O_2, and k_{cat}, C_o, and t are the catalytic rate constant (M^{-1} s^{-1}), catalyst concentration (M) and time elapsed (s), respectively. For a small time range, the values of I_{cat}/I_L are linear with respect to $t^{1/2}$ (not shown). From the slope of the I_{cat}/I_L vs. $t^{1/2}$ plot, we can simply calculate the value of k_{cat} for a given concentration of analyte. The value of k_{cat} for a chemical reaction of H_2O_2 at a PBNP-GCE-red was found to be 1.7×10^5 cm^3 mol^{-1} s^{-1}.

Electrocatalytic reduction of H_2O_2 at the PBNP-GCE-red

To reveal the electrocatalytic activity of PBNPs, the voltammetric behavior of H_2O_2 was investigated at the surface of PBNP-GCE-red. Figure 4 illustrates the cyclic voltammograms of the PBNP-GCE-red in the absence (dotted line) and presence (solid line) of H_2O_2 in a solution of 0.1 M KCl (pH = 4). The symmetrical redox peaks related to the PBNP-modified electrode were changed by the addition of H_2O_2. The catalytic action of PW, produced by the electrochemical reduction of PB at the electrode surface, towards H_2O_2 reduction can be described as follows:

$$Fe_4\left[Fe(CN)_6\right]_3 + 4K^+ + 4e^- \rightarrow K_4Fe_4\left[Fe(CN)_6\right]_3$$

$$K_4Fe_4\left[Fe(CN)_6\right]_3 + 2H_2O_2 + 4H^+ \\ \rightarrow Fe_4\left[Fe(CN)_6\right]_3 + 4H_2O + 4K^+$$

In addition, Fig. 5 shows the cyclic voltammograms of the PBNP-GCE-red were recorded at different scan rates in the presence of 0.05 mM H_2O_2. This survey showed that the reduction current (I_{pc}) increased linearly with the square root of the scan rate ($v^{½}$) (inset (a) in Fig. 5a), which could be related to the slow diffusion of potassium ions into the PBNS lattice. Furthermore, a plot of the peak current ratio ($I_{pc}/v^{½}$) vs. v exhibits an indicative shape typical of an EC′ catalytic process, as shown in inset b to Fig. 5b.

For an electroactive material with a diffusion coefficient D, the current response under condition of diffusion control is described by Cottrell equation [47] $I = nFACD^{1/2}/(\pi t)^{1/2}$. Where n is the number of electrons; F is the Faraday constant; A is the electrode area; C is the bulk concentration of analyte; D is the diffusion coefficient of analyte in solution; t is the time. In that case, D can be determined from the slope of I–$t^{-1/2}$ curve. The average diffusion coefficient of iodide was calculated to be 2.6×10^{-5} cm^2 s^{-1}. In addition, The apparent Michaelis–Menten constant (K_M^{app}), which gives an indication of the enzyme-substrate kinetics, can be calculated from the electrochemical version of the Lineweaver–Burk equation $\frac{1}{I_{ss}} = \frac{1}{I_{max}} + \frac{K_M^{app}}{I_{max} C}$, where I_{ss} is the steady-state current after the addition of substrate, C is the bulk concentration of the substrate and I_{max} is the maximum current measured under saturated substrate condition. The K_M^{app} was determined by analysis of the slope and intercept for the plot of the current versus H_2O_2 concentration. The K_M^{app} value of the H_2O_2 sensor was determined by steady-state amperometric response and found to be 0.021 μM.

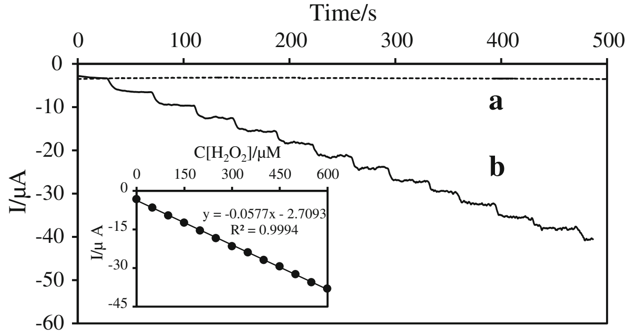

Fig. 6 The current–time profiles obtained at the PBNP-GCE-red under continuous stirring conditions during the successive addition of H_2O_2 in the range 0–600 μM (**a**). The calibration graph derived from the current–time profiles (**b**)

The amperometry experiment was carried out at different concentrations of H_2O_2. Figure 6a shows typical current–time responses for the successive addition of H_2O_2. The sensor responds rapidly to the substrate, as about 95 % of the steady-state current is obtained within 6 s. The inset to Fig. 6b shows a plot of catalytic current, which changes linearly with the H_2O_2 concentration in the range of 50–600 μM. The linear regression equation of the calibration curve is expressed as I (μA) = −0.0577C [H_2O_2] (μM) −2.7 with a correlation coefficient of 0.9994 ($n = 13$). The detection limit of the proposed electrode was found to be 0.51 μM (S/N = 3). The comparisons of electrocatalytic characteristics of PBNP-GCE-red based H_2O_2 sensor with different MHCF-modified electrode are summarized in Table 1. It can be seen that the detection limit of this proposed method is lower than GE/PBNPs/Nafion and PBNP-modified CCE for the determination of H_2O_2, but also higher than GO/PB. Moreover, the electrocatalytic properties of PBNP-GCE-red are comparable with sol–gel HRP-modified enzyme electrode [49].

Figure S4 shows the calibration curves obtained for amperometric detection of H_2O_2 performed at porous glassy carbon electrodes with different number of PB layers. PBNP-GCE-red with six deposition cycles displayed the highest sensitivity. It could be attributed to the difficult electron transfer and penetration of the counter ion (K^+) and also, blocked diffusion of H_2O_2 with the increasing film deposition cycles.

The interferences of typical organic compounds such as dopamine (DA), uric acid (UA) and ascorbic acid (AA), and, during amperometric sensing of H_2O_2, were also studied at the PBNP-GCE-red (Fig. S5). The current responses generated due to these interfering species are negligible for (DP and UA), but a 3.1 % error criterion was

Table 1 A comparison of this work with other modified electrode based on MHCF

Modified electrode	E_{app} (mV)	LOD (μM)	LDR (μM)	pH of solution	Sensitivity (mA M^{-1} cm^{-2})	Ref.
GO/PB	100[a]	0.12	5–1,200	6	408.7	[32]
PB@Ptnano/carbon nanotubes	100[b]	0.15	0.25–1,500	2	850	[33]
GE/PBNPs/Nafion	−50[b]	1	2.1–140	7	138.6	[34]
GCE/CuHCFe/PPy	0[a]	14	0–500	1	726	[35]
PBNP-modified CCE	−100[a]	0.78	0–500	4	754.6	[36]
SnHCF|CCE	−100[a]	1.47	4–50	4	588	[37]
CuHCFe-CILPE	−50[b]	0.9	1–1,000	7	39.8	[38]
PBNP-GCE-red	−100[b]	0.51	0–600	4	333	This work

[a] vs. SCE

[b] vs. Ag|AgCl

E_{app} applied potential, *LDR* linear dynamic range, *LOD* detection of limit, *GO* grapheme oxide, *GE* graphite electrode, *PPy* polypyrrole, *CCE* carbon ceramic electrode, *SnHCF* tin hexacyanoferrate, *CuHCFe-CILPE* copper hexacyanoferrate modified carbon ionic liquid paste electrode

adopted for (AA), indicating high selectivity of the sensor. In addition, repetitive redox cycling experiments were done to determine the extent of stability relevant to PBNP-GCE-red in 0.1 M KCl solution (pH = 4). After 30 continuous cycles at 50 mVs^{-1}, the peak heights of the cyclic voltammograms did not show considerable decrease (not shown).

Conclusions

In this study, the nano porous glassy carbon electrode has been applied as the support for the immobilization of Prussian blue nanocubic particles based on self-assembly technique for fabrication of hydrogen peroxide sensor. The kinetics of the catalytic reaction has been explained using cyclic voltammetry and amperometry. The experimental results demonstrate that the proposed sensor exhibited good sensitivity, high stability, fast response and anti-interference ability for electrocatalytic reduction of H_2O_2.

Acknowledgments The author thanks Dr P. Marashi and Miss somayeh jalilzadeh from Maharfan Abzar Co (Tehran, Iran) for the support with the AFM system. We would like to thank Dr. Behzad Haghighi for all his advice.

References

1. R. Pauliukaite, M. Florescu, C.A. Brett, J. Solid State Electrochem. **9**, 354 (2005)
2. U. Scharf, E.W. Grabner, Electrochim. Acta **41**, 233 (1996)
3. M.S. Lin, T.F. Tseng, Analyst **123**, 159 (1998)
4. W. Costa, A.E.B. Marques, E. Marques, C.B. Bezerra, E. Sousa, W. Cardoso, C. Song, J. Zhang, J. Appl. Electrochem. **40**, 375 (2010)
5. A. Abbaspour, A. Khajehzadeh, A. Ghaffarinejad, J. Electroanal. Chem. **631**, 52 (2009)
6. H. Razmi, R. Mohammad-Rezaei, Electrochim. Acta **55**, 1814 (2010)
7. X.-Q. Zhang, S.-W. Gong, Y. Zhang, T. Yang, C.-Y. Wang, N. Gu, J. Mater. Chem. **20**, 5110 (2010)
8. A.K. Dutta, S.K. Maji, D.N. Srivastava, A. Mondal, P. Biswas, P. Paul, B. Adhikary, J. Mol. Catal. A: Chem. **360**, 71 (2012)
9. L. Wang, E. Wang, Electrochem. Commun. **6**, 225 (2004)
10. E.S. Forzani, G.A. Rivas, V.M. Solis, J. Electroanal. Chem. **382**, 33 (1995)
11. S. Hrapovic, Y. Liu, K.B. Male, J.H.T. Luong, Anal. Chem. **76**, 1083 (2003)
12. J. Shen, X. Yang, Y. Zhu, H. Kang, H. Cao, C. Li, Biosens. Bioelectron. **34**, 132 (2012)
13. X. Bo, J. Bai, J. Ju, L. Guo, Anal. Chim. Acta **675**, 29 (2010)
14. C.-L. Hsu, K.-S. Chang, J.-C. Kuo, Food Control **19**, 223 (2008)
15. Y.-C. Weng, K.-C. Hung, Sens. Actuators B: Chem. **141**, 161 (2009)
16. C. Debiemme-Chouvy, Biosens. Bioelectron. **25**, 2454 (2010)
17. S.A. Kumar, S.-M. Chen, J. Mol. Catal. A: Chem. **278**, 244 (2007)
18. J. Wang, R. Yuan, Y. Chai, W. Li, P. Fu, L. Min, Colloids Surf. B **75**, 425 (2010)
19. L. Wang, H. Zhu, Y. Song, L. Liu, Z. He, L. Wan, S. Chen, Y. Xiang, S. Chen, J. Chen, Electrochim. Acta **60**, 314 (2012)
20. Y. Liu, R. Yuan, Y. Chai, D. Tang, J. Dai, X. Zhong, Sens. Actuators B: Chem. **115**, 109 (2006)
21. Z. Cao, X. Jiang, Q. Xie, S. Yao, Biosens. Bioelectron. **24**, 222 (2008)
22. F. Gao, Z. Yao, Q.a. Huang, X. Chen, X. Guo, Q. Ye, L. Wang, Colloids Surf. B **82**, 359 (2011)
23. X.X. Xu, J.X. Zhang, F. Guo, W. Zheng, H.M. Zhou, B.L. Wang, Y.F. Zheng, Y.B. Wang, Y. Cheng, X. Lou, B.Z. Jang, Colloids Surf. B **84**, 427 (2011)
24. K. Zhou, Y. Zhu, X. Yang, J. Luo, C. Li, S. Luan, Electrochim. Acta **55**, 3055 (2010)
25. J. Jia, B. Wang, A. Wu, G. Cheng, Z. Li, S. Dong, Anal. Chem. **74**, 2217 (2002)
26. A.A. Karyakin, E.E. Karyakina, Sens. Actuators B: Chem. **57**, 268 (1999)
27. M.P. O'Halloran, M. Pravda, G.G. Guilbault, Talanta **55**, 605 (2001)
28. A.A. Karyakin, E.A. Puganova, I.A. Budashov, I.N. Kurochkin, E.E. Karyakina, V.A. Levchenko, V.N. Matveyenko, S.D. Varfolomeyev, Anal. Chem. **76**, 474 (2003)
29. I.L.d. Mattos, L. Gorton, T. Ruzgas, A.A. Karyakin, Anal. Sci. **16**, 795 (2000)
30. F. Ricci, C. Gonçalves, A. Amine, L. Gorton, G. Palleschi, D. Moscone, Electroanalysis **15**, 1204 (2003)
31. A. Malinauskas, R. Araminait, G. Mickeviciut, R. Garjonyt, Mater. Sci. Eng. C **24**, 513 (2004)
32. A.A. Karyakina, O.V. Gitelmachera, E.E. Karyakinaa, Anal. Lett. **27**, 2861 (1994)
33. N.F. Zakharchuk, B. Meyer, H. Henning, F. Scholz, A. Jaworksi, Z. Stojek, J. Electroanal. Chem. **398**, 23 (1995)
34. M. Pyrasch, A. Toutianoush, W. Jin, J. Schnepf, B. Tieke, Chem. Mater. **15**, 245 (2002)
35. S. Lupu, C. Mihailciuc, L. Pigani, R. Seeber, N. Totir, C. Zanardi, Electrochem. Commun. **4**, 753 (2002)
36. Y. Guo, A.R. Guadalupe, O. Resto, L.F. Fonseca, S.Z. Weisz, Chem. Mater. **11**, 135 (1998)
37. N.R. de Tacconi, K. Rajeshwar, R.O. Lezna, Chem. Mater. **15**, 3046 (2003)
38. M. Ferreira, P.A. Fiorito, O.N. Oliveira Jr, S.I. Córdoba de Torresi, Biosens. Bioelectron. **19**, 1611 (2004)
39. Z. Xu, N. Gao, H. Chen, S. Dong, Langmuir **21**, 10808 (2005)
40. Y. Liu, Z. Chu, W. Jin, Electrochem. Commun. **11**, 484 (2009)
41. P.A. Fiorito, V.R. Goncales, E.A. Ponzio, S.I.C. de Torresi, Chem. Commun. **0**, 366 (2005)
42. J.-D. Qiu, H.-Z. Peng, R.-P. Liang, J. Li, X.-H. Xia, Langmuir **23**, 2133 (2007)
43. Q. Wang, L. Zhang, L. Qiu, J. Sun, J. Shen, Langmuir **23**, 6084 (2007)
44. Q.-L. Zhao, Z.-L. Zhang, L. Bao, D.-W. Pang, Electrochem. Commun. **10**, 181 (2008)
45. Q.-L. Zhao, Z.-L. Zhang, L. Bao, D.-W. Pang, Electrochem. Commun. **10**, 181 (2008)
46. J. Wang, *Analytical electrochemistry* (VCH, New York, 1994)
47. L.R.F.A.J. Bard, *Electrochemical methods, fundamentals and Applications* (Wiley, New York, 1980)
48. Z. Galus, *Fundamentals of electrochemical analysis (Ellis Horwood series in analytical chemistry* (Ellis Horwood Press, New-York, 1976)
49. J. Li, S.N. Tan, H. Ge, Anal. Chim. Acta **335**, 137 (1996)